

NeoCASS: an integrated tool for structural sizing, aeroelastic analysis and MDO at conceptual design level

L. Cavagna ^{*}, S. Ricci [†] and L. Travaglini [‡]

This paper presents a design framework called NeoCASS (Next generation Conceptual Aero-Structural Sizing Suite), developed at the Department of Aerospace Engineering of Politecnico di Milano in the frame of SimSAC (Simulating Aircraft Stability And Control Characteristics for Use in Conceptual Design) project, funded by EU in the context of 6th Framework Program. It enables the creation of efficient low-order, medium fidelity models particularly suitable for structural sizing, aeroelastic analysis and optimization at the conceptual design level. The whole methodology is based upon the integration of geometry construction, aerodynamic and structural analysis codes that combine depictive, computational, analytical, and semi-empirical methods, validated in an aircraft design environment. The result is a design tool based on computational methods for the aero-structural analysis and multi disciplinary optimization (MDO) of aircraft layouts at the conceptual design stage. A complete case study regarding the TransonicCRuiser aircraft, including validation results obtained using industrial standard tools like MSC/NASTRAN and medium fidelity CFD codes like Edge, is also reported.

Nomenclature

α	Angle of attack
δ_c	Canard deflection
α_T	Angle of attack at trim condition
δ_T	Canard deflection at trim condition
Δs	Structural node displacement
$\Delta\theta$	Structural node deflection
λ	Eigenvalue
Ψ	Mode shapes
\mathbf{q}	Modal amplitudes
CG	Center of gravity
MAC	Mean Aerodynamic Chord
CN_0	Normal aerodynamic force coefficient at the reference condition
Cm_0	Pitch moment coefficient at the reference condition
$CN(\cdot)$	Normal aerodynamic force coefficient derivative w.r.t. (\cdot)
$Cm(\cdot)$	Pitch moment coefficient derivative w.r.t. (\cdot)
z	Altitude
k	Reduced frequency
M_∞	Free stream Mach number

^{*}Scientist, Ph.D., FOI - Swedish Defence Research Agency, Stockholm - Sweden, Luca.Cavagna@foi.se

[†]Associate Professor, Dipartimento di Ingegneria Aerospaziale, Politecnico di Milano - Italy, Sergio.Ricci@polimi.it.

[‡]M.Sc. student, Dipartimento di Ingegneria Aerospaziale, Politecnico di Milano - Italy, Lorenzo.Travaglini@mail.polimi.it.

\mathcal{P}_{M_a}	Flight mechanics accelerations
\mathcal{P}_{M_c}	Flight mechanics control parameters
\mathcal{P}_{M_e}	Elastic parameters
\mathcal{P}_{M_v}	Flight mechanics parameters
q_∞	Free stream dynamic pressure
V_∞	Free stream velocity

I. Introduction

Most of the life-cycle cost of an aircraft is incurred during the conceptual design phase and therefore, the earlier an appropriate conceptual configuration can be found, the more economical the whole design process will be, avoiding costly later redesign and corrections. Contemporary commercial aircraft conceptual design tools make extensive use of handbook methods based on semi-empirical theory and data. In particular, during conceptual design phase, statistical based approaches are adopted for structural weight estimation, like ones reported in.^{1,2} Nevertheless, it appears as quite unreliable to adopt statistical-based approaches where no enough knowledge is available, as in case of unconventional configurations and new technologies such as for example Sensorcraft^{3,4} and Blended Wing Body aircraft.⁵ The use of statistical based approaches for the structural weight estimation means that the aircraft structure is practically absent till the preliminary design phase. Due to this choice, it is almost impossible to take into consideration aeroelastic requirements that in fact appear later during the design loop. Unfortunately, new transport aircraft are very flexible and aeroelastic effects must be taken into consideration right from the beginning of the design phase so to avoid very expensive redesign during preliminary design phase or resulting weight penalties needed to satisfy aeroelastic requirements not previously taken into account. Recently, new software systems specifically tailored for aircraft conceptual design have been proposed⁶ but while they include specific tools for taking into account of different aspects and requirements, such as ones coming from environmental impact, the capabilities of considering more realistic structural models are still missing. In some cases statistical-based approaches are substituted by deriving structural weight prediction based on single loading parameter, like the root wing bending. On the other hands, specific methods based on semi-analytical approach have been developed mainly to enhance the weight prediction capabilities^{7,8} but in many cases they are specific modules not included into a more general aircraft conceptual design framework, including aircraft performances and stability and control. The need for aeroelastic analysis capability within SimSAC project has led to the development of a completely new specialised module called NeoCASS (Next Generation Conceptual Aero-Structural Sizing Suite) to perform structural sizing, aeroelastic analysis and optimization. The following pages report a detailed description of NeoCASS module.

II. Layout of NeoCASS

NeoCASS (*Next generation Conceptual Aero Structural Sizing*) is a suite of modules that combines state of the art computational, analytical and semi-empirical methods to tackle all the aspects of the aero-structural analysis of a design layout at conceptual design stage. It gives a global understanding of the problem at hand without neglecting any aspect of it: weight estimation, initial structural sizing, aerodynamic performances, structural and aeroelastic analysis from low to high speed regimes, divergence, flutter analysis and determination of trimmed condition and stability derivatives both for the rigid and deformable aircraft. More specifically, NeoCASS includes two main modules, named GUESS (*Generic Unknowns Estimator in Structural Sizing*) and SMARTCAD (*Simplified Models for Aeroelasticity in Conceptual Aircraft Design*), respectively, while is linked to a third module, called W&B (*Weight and Balance*), used also by other modules of CAESIOM procedure.

In order to start aeroelastic analysis, a semi-analytical module named GUESS (*Generic Unknowns Es-*

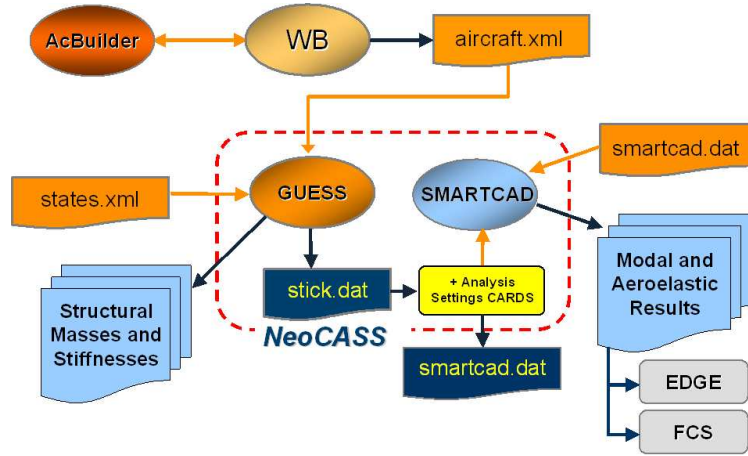


Figure 1: NeoCASS layout.

*timator in Structural Sizing), based on a modified version of the AFaWWE code (*Analytical Fuselage and Wing Weight Estimation*),⁹ is run just to produce a first-try stiffness distribution. The first trial structural sizing is performed in a fully stressed design condition but taking into account of structural instability limits related to compressed panels and stiffeners. In this structural sizing phase, no aeroelastic effects are considered. Once completed the initial structural sizing and the first stiffness distribution is determined, the GUESS module automatically generates the structural and aerodynamic mesh for the following aeroelastic analysis assessed by means of a dedicated aeroelastic module named SMARTCAD (*Simplified Models for Aeroelasticity in Conceptual Aircraft Design*). NeoCASS includes also a dedicated Multi-Disciplinary Optimization (MDO) tool used to refine the initial structural sizing in order to satisfy the aeroelastic constraints which can be expressed as limits on: divergence speed, aeroelastic stability derivatives, maximum deformed shape under loading due to structural flexibility, flutter speed, keeping the aircraft geometry as fixed. In this way, it is possible to consider specific aeroelastic requirements that cannot be taken into account during the initial estimation of stiffness distribution done by GUESS module.*

The starting point to run a NeoCASS session is the XML file including all the aircraft properties. This file can be easily generated using AcBuilder, a dedicated module that has been developed to make the aircraft definition process easy for typical user.

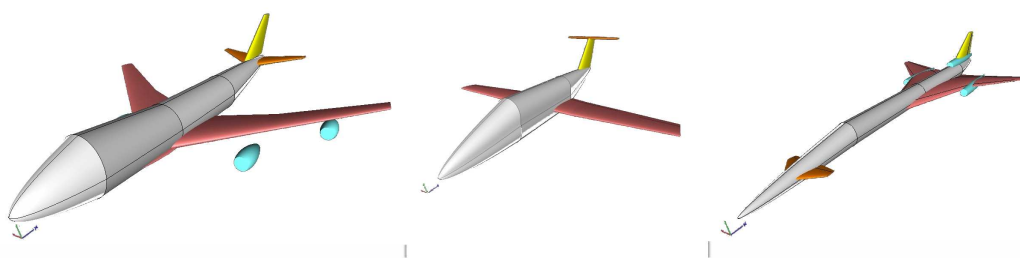


Figure 2: Samples of parametric geometry models.



Figure 3: NeoCASS Graphical User Interface.

Geometry parameters together with geometry derived variables, e.g. area, mean chord, leading edge, quarter chord sweep, are stored into an unique file named *aircraft.xml*, including also structural concepts and material properties adopted by GUESS during initial structural sizing, after which a first estimate of the structural weight and stiffness distribution is available.

A stick mesh model with all elements connectivity, material properties, non-structural lumped masses coming from WB is exported to the ASCII file *stick.dat* to be used by the solver SMARTCAD for aero-structural analyses. Further parameters are provided as setting cards to the solver to determine and rule the analysis to be carried out. When the parameters are combined to the mesh file, a *smartcad.dat* file is available which can be independently re-used and modified by the designer to carry out the simulation required using SMARTCAD as a stand-alone application. Several outputs are finally available to the structural engineer for post-processing purposes, e.g. stresses, displacements, and to the other modules, e.g. stability derivatives, trimmed polars, vibration modes for flight-dynamic simulations including aeroelastic effects, under the hypothesis of small structural displacements. A user friendly Graphical User Interface (GUI) has been developed allowing for an easy access to all NeoCASS software modules for model preparation, analysis and results post-processing (See Figure 3).

III. Initial structural sizing using GUESS

A method based on fundamental structural principles for estimating the load-bearing airframe for fuselage and lifting surfaces is adopted for GUESS module. This method is particularly useful for the weight estimation of aircraft at conceptual level since it represents a compromise between the rapid assessment of component weight using empirical methods, based on actual weights of existing aircraft, and detailed but time-consuming finite-element analysis. The present work starts from the work originally performed by Ardema et al.⁹ extending it to the sizing of horizontal and vertical tail planes to have a complete view of the whole airframe. The distribution of loads and vehicle geometry is accounted for, since the analysis is done station-by-station along the vehicle longitudinal axis and along the lifting surface structural chord, giving an integrated weight which depends on local conditions and structural concepts adopted.

Two are the strategies implemented into GUESS module, briefly summarized in Figure 4(b), based on the use of standard pre-defined maneuvers (GUESS in Standard mode) or user-defined maneuvers (GUESS in Modified mode). The standard pre-defined maneuvers are pull-up at prescribed normal load, landing, bump on irregular runway, and rudder maximum deflection and depend on the design specifications (for example maximum load factor, landing sink velocity, differential pressure inside the fuselage). Specific lateral maneuvers according to FAR-25 criteria are considered to improve the accuracy of vertical tail sizing, i.e. abrupt rudder maneuvers and engine-out sideslip flight. To estimate some of the key lateral directional analysis, including stability and control derivatives for use in estimating aircraft characteristics, the approach proposed by Mason¹⁰ is adopted.

When using GUESS in Modified mode the design maneuvers can be easily prescribed by the user by defining the complete state vector: both symmetric and asymmetric maneuvers can be specified without any limitation on their total number. Once the loads are defined, the sizing is performed for each station

under the constraints of ultimate compressive and tensile strength, local and global buckling and minimum gage. In particular, principles of minimum weight can then be used such that, given an applied load and the limitations on the outside dimensions, the most efficient type of construction, its geometry and material are directly determined.^{11, 12, 9}

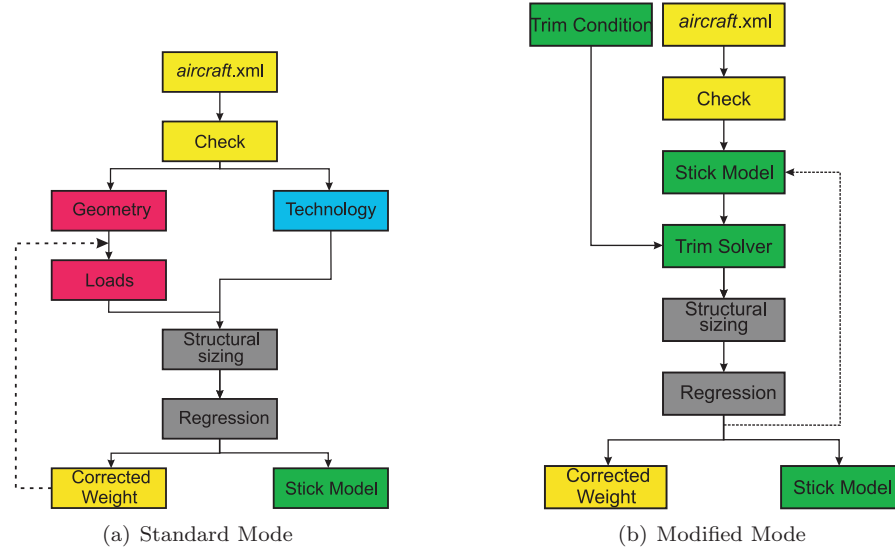


Figure 4: Block diagram of GUESS in Standard (left) and Modified (right) mode.

At the end of the sizing process, GUESS automatically generates a stick beam model for SMARTCAD by means of a semi-monocoque method. Figure 5 shows some details of the typical model generated.

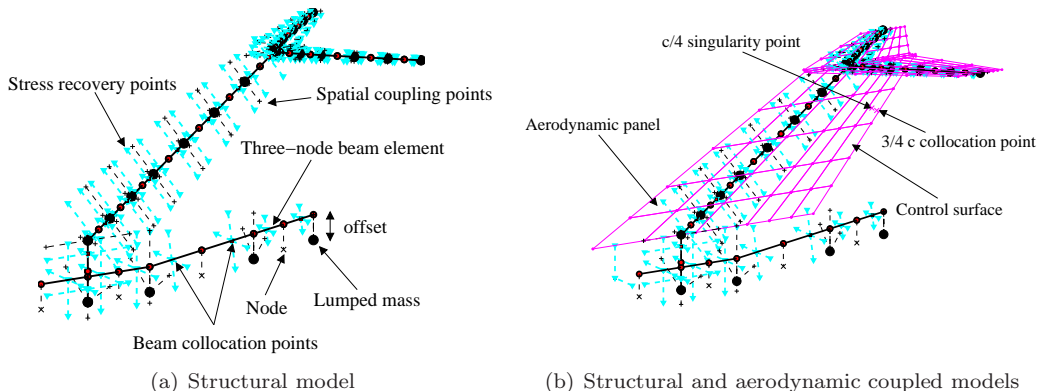


Figure 5: Nomenclature for the aeroelastic model.

Besides exporting mechanical properties and the basic stick model, extra information are given:

- stress-recovery points along the sides of the wing-box and fuselage where stresses are calculated;
- extra-nodes perpendicular to the beam axis and simply connected to beam nodes through rigid elements (hypothesis of beam model implying rigid section); they instantaneously enable to visualize the twist

rotational motion of the boundaries of the wing-box and are mainly be used for the coupling with the aerodynamic model to transfer forces and displacements.

when the beam stick model is automatically generated, all non-structural masses are correctly introduced in the structural mesh as: lumped non-structural masses on mesh nodes (engines, landing gears, auxiliary tanks, systems) and non-structural densities per unit length along the beams (passengers in fuselage, fuel in wings, paint, furniture). The aerodynamic mesh created allows to be indistinguishably used for classic lifting surface panel methods such as Vortex Lattice,¹³ Vortex Ring,¹⁴ Doublet Lattice¹⁵ and Harmonic Gradient.¹⁶ Wing-box dimensions, internal volume of fuel available and chord-wise camber distribution are simply determined once the airfoil used at different spanwise control sections is defined. Finally, considering the early design phase the framework is intended for, control surfaces are currently represented by their aerodynamic contributions, neglecting their inertia, dynamics and actuation systems.

IV. Aeroelastic Analysis Using SMARTCAD

SMARTCAD is the numerical module of NeoCASS dedicated to aero-structural analysis. It can be used as a stand-alone application once the structural and aerodynamic meshes are provided, together with solver parameters. Different kind of analysis can be carried out:

- static analysis, linear buckling.
- vibration modes calculations
- linearized flutter analysis;
- linear/non-linear static aeroelastic analysis, trimmed calculation for a free-flying rigid or deformable aircraft;
- steady and unsteady aerodynamic analysis to extract derivatives for flight mechanics applications;
- structural optimization.

At the moment structural beam models, based on a three-node linear/non linear finite-volume beam which proved to be intrinsically shear-lock free,¹⁷ and classic lifting aerodynamic surfaces are heavily used, despite the code can be coupled to high fidelity aerodynamic models belonging to the class of Computational Fluid Dynamics (CFD). Two class of methods are available for this purpose within SMARTCAD: an innovative scheme, based on Moving Least Square (MLS) method (see Quaranta et al.¹⁸) and the Radial Basis Function (RBF) method (see Beckert and Wendland¹⁹), both methods ensuring the conservation energy transfer between the fluid and the structure and they are suitable for the treatment of complex configurations. To avoid interpolating rotations and using the same algorithms in a straightforward way also for CFD meshes, extra points are added along the wingbox through rigid-arms. Aerodynamic loads are distributed along both master beam nodes and these additional nodes. Loads are then reduced to lumped forces and moments on the former set of nodes.

IV.A. Optimization Module

The first structural sizing on minimum weight principles according to strength criteria on ultimate loads, obtained using GUESS, must be considered to be a good starting point for stiffness and inertia distribution, when the aeroelastic analysis highlight unsatisfied aeroelastic requirements and the need for a structural optimization arises. Thus, a simple optimization process based on Gradient-based Optimization Methods can be adopted to slightly modify the airframe so that aeroelastic requirements are satisfied as well. The

classic statement for the problem of constrained optimization reads:

$$\begin{aligned} \text{minimize : } & I(d_j) \\ \text{with respect to : } & d_j, \quad j = 1, 2, \dots, N_d \\ \text{subject to : } & g_m(d_j) \geq 0, \quad m = 1, 2, \dots, N_g \end{aligned}$$

where I is a non-linear function of the design variables d_j and g_m are the non-linear constraints to be satisfied. The parameters are allowed to vary in a limited design space to guarantee a feasible and realistic solution such that the design features the best figure of merit. Optimization algorithms are supposed to perform such task in a rigorous way. Many methods are available and the literature on this topic is large, see for example.²⁰ A well known category is the gradient-based one which uses the value of the objective function and its gradients with respect to the design variables where the sensitivity information is used to determine iteratively the new design variables. In the present work, the Feasible Direction Method has been adopted. During the optimization process, the objective and the constraints must be repeatedly evaluated, raising the overall computational cost since each evaluation demands for a numerical simulation. A common approach consists in creating an approximated linearized problem and feed the optimizer with such simplified model. This results in a very relatively inexpensive process. MDO module implemented into SMARTCAD adopts an approximate model based on the convex linearization technique.

V. Interfacing NeoCASS with Medium Fidelity Tools Based on CFD

The strategy adopted inside SimSAC project and during the development of NeoCASS module was based on the concept of multi-fidelity aerodynamic modeling, as follows:

- Tier 1 tools, based on VLM/DLM solvers used for steady and unsteady aerodynamic calculations. These tools have been derived from available code (like Tornado from KTH) or developed from scratch, like the DLM solver. Both these tools are completely embedded into NeoCASS and can be adopted by the user during the conceptual design phase;
- Enhanced Tier 1 tools, based on FOI-Edge URANS code. In this case the CFD solver is not embedded into NeoCASS but the ROM models created using it can be easily imported and used during NeoCASS runs.

The reason for this approach is well known. The strong nonlinearities associated to shock waves in transonic flows require the adoption of non-isentropic flow-models based of the Euler or Navier-Stokes equations. Classic linear(ised) potential theories are not able to model the non-linear physics associated with shock waves, leading to wrong predictions of both steady and unsteady pressure load distributions with consequent gross mistakes in the performances of the aeroelastic system. Despite their inaccuracy in the transonic regime, classical models based on unsteady potential flow are still heavily used with possibly empirical corrections; unfortunately this requires the knowledge of experimental results and additional work to adjust the numerical model and thus does not go well with the CEASIOM environment purposes. As pointed out by Bennet and Edwards,²¹ significant improvements, still undeniable nowadays, are required to allow a more extensive routine usage of CA based on CFD models. They include:

- reduction of computational times;
- increase of CFD tools credibility for unsteady simulations;
- simplification of the procedures for a more effective application during the design and verification phases.

The first and third requirements have been clearly recognized by the SimSAC project and were object of dedicated work packages. The second need distinguishes a foundation and simultaneously a challenge of the SimSAC project: the target of enhancing the conceptual design with low-to-high fidelity tools to be First Time Right. Inviscid analysis are carried out by the means of the traspiration wall boundary condition introduced in one of next paragraph. This guarantees a good trade-off between accuracy in the transonic regime and the computational costs which must be kept as low as possible since several configuration are to analized in CEASIOM environment during the optimization loop. Moreover the issues related to grid deformation and element distortion, which can dangerously stop the CFD solver in cases of grid invalidations, are avoided.

VI. Trim process using the CFD solver

The quest for the trim configuration requires the solution of a non-linear system of equations that implicitly involves those constituting the CFD model as well. When structural displacements are considered, the trim solution can be obtained by considering a single non-linear system of equations \mathcal{F} , composed by the flight mechanics \mathcal{F}_R and the structural \mathcal{F}_E equations. This system depends on two sets of parameters: the free-stream parameters, i.e. dynamic pressure q_∞ and Mach number^a, and the configuration parameters \mathcal{P}_M , which can be modified during the trim procedure. The configuration parameters can be additionally subdivided into four fundamental sets:

- flight mechanics configuration, i.e. the angle of attack, the side-slip angle and the angular velocities, $\mathcal{P}_{M_v} = [\alpha, \beta, p, q, r]^T$;
- flight mechanics accelerations, i.e. load factors along the three different coordinate axis plus the angular acceleration $\mathcal{P}_{M_a} = [n_x, n_y, n_z, \dot{p}, \dot{q}, \dot{r}]^T$;
- control parameters, composed by the deflection of all control surfaces and the engine thrust $\mathcal{P}_{M_c} = [\delta_a, \dots, T]^T$;
- the elastic parameters composed by the flexible mode amplitudes $\mathcal{P}_{M_e} = \mathbf{q}^T$.

The objective in this work is the development of an efficient tool for static aeroelasticity of maneuvering aircraft able to include nonlinear aerodynamic effects. The tool is specifically intended for the early design process, allowing to efficiently evaluate the structural design loads, aerodynamic derivatives modification due to aeroelastic effects and, eventually, flutter boundaries.

To reduce the size and the complexity of the problem and being not interested in the elastic stresses in the structure, the structural model is represented by a reduced model based on its normal vibration modes, available from NeoCASS, instead of the complete FE model. This does not affect substantially the quality of the final aimed results, as with normal modes the structural displacements, which are the only cause of modification for aerodynamic loads, converge quickly to the correct values by increasing the number of modes. Such approach has been shown to be adequate in various linear static aeroelastic analysis.²² The solution is required to be applicable to free-free aircraft, including inertia relief effects to allow a trim solution for a prescribed load factor. In this respect, the adoption of normal modes as generalized coordinates enables to automatically consider such effects without having to apply inertia relief techniques to circumvent the singularity in the stiffness matrix \mathbf{K} . The trim problem can be stated as

$$\mathcal{F}(q, \text{Ma}, \mathcal{P}_M) = \begin{cases} \mathcal{F}_R(q_\infty, \text{Ma}_\infty, \mathcal{P}_{M_v}, \mathcal{P}_{M_a}, \mathcal{P}_{M_c}, \mathcal{P}_{M_e}) = 0, \\ \mathcal{F}_E(q_\infty, \text{Ma}_\infty, \mathcal{P}_{M_v}, \mathcal{P}_{M_a}, \mathcal{P}_{M_c}, \mathcal{P}_{M_e}) = 0. \end{cases} \quad (1)$$

^aDependency from the Reynolds number should be considered in principles. However, for this specific case since it has been decided to adopt a simpler Euler model for the fluid flow, the dependency from Reynolds is neglected.

The flight mechanics equations are equal to

$$\begin{bmatrix} m\mathbf{I} & -\mathbf{S} \\ -\mathbf{S}^T & \mathbf{J} \end{bmatrix} \begin{Bmatrix} \mathbf{n}g \\ \dot{\boldsymbol{\omega}} \end{Bmatrix} = q_\infty \mathbf{f}_a^R(\mathbf{Ma}_\infty, \mathcal{P}_{M_v}, \mathcal{P}_{M_a}, \mathcal{P}_{M_c}, \mathcal{P}_{M_e}), \quad (2)$$

where m is the aircraft mass, \mathbf{S} is the matrix of statical moments of inertia, \mathbf{J} is the matrix of moments of inertia, \mathbf{n} is the vector of load factors, g is the gravity acceleration, $\boldsymbol{\omega} = [p, q, r]^T$ is the vector of angular velocities, and \mathbf{f}_a^R is the vector of GAFs on rigid body modes divided by q . Whereas, the elastic equations for the trim problem are

$$\mathbf{K}\mathbf{q} = q\mathbf{f}_a^E(\mathbf{Ma}, \mathcal{P}_{M_v}, \mathcal{P}_{M_a}, \mathcal{P}_{M_c}, \mathcal{P}_{M_e}). \quad (3)$$

The GAFs provide the only coupling between the flight mechanics and the elastic structural equations; no inertial coupling has to be considered since normal modes of an unrestrained structure are by definition mean-axes modes.²³ For the same reason, no effect of gravity on elastic equations must be considered.

The system of equations composed by Eqs. (2)–(3) cannot be solved immediately for all the M configuration parameters, because they usually exceed the number of equations ($N + 6$), with N the number of elastic modes. ($M - N - 6$) configuration parameters need to be set *a priori* in order to define the type of maneuver under investigation, such as cruise, symmetric pull-up, turn and so on. The resulting problem is usually referred as a *consistent aeroelastic problem*. As a matter of fact, the deformation parameters \mathbf{q} are always among the unknowns of the problem, because the steady deformed condition is never assigned in a maneuvered flight. Additionally, in the present work only five flight mechanics equations are used, because the equilibrium equation along the drag direction is always considered satisfied under the hypothesis of sufficient thrust available for the required maneuver. So, the number of equations for the rigid motion is lowered to five and n_x and T are never included in the configuration set. On the other hand, when a consistent solution cannot be formulated, the trim problem can be cast into an optimization problem, as shown in.^{24,25}

Generally speaking, the resulting system of equations is nonlinear and thus requires dedicated iterative numerical methods to be solved. If a classical Newton method is adopted, the trim is found as result of an iterative process which requires the solution of a sequence of linear systems

$$\mathbf{J}_m(\mathcal{P}_M^k)\delta\mathcal{P}_M^k = -\mathcal{F}(\mathcal{P}_M^k), \quad \mathcal{P}_M^{k+1} = \delta\mathcal{P}_M^k + \mathcal{P}_M^k, \quad k = 0, 1, \dots \quad (4)$$

The Jacobian matrix $\mathbf{J}_m = \frac{\partial \mathcal{F}}{\partial \mathcal{P}_M}$ cannot be easily evaluated analytically so, an efficient numerical approach must be introduced. Under the hypothesis of small structural deformations, it may be convenient to adopt a staggered approach, applying the Newton algorithm first to the rigid equilibrium equations \mathcal{F}_R while keeping the modal amplitudes fixed, and then to the elastic equations \mathcal{F}_E . In this way the evaluation of the Jacobian matrix is simplified, since it is implicitly assumed that

$$\frac{\partial \mathcal{F}_R}{\partial \mathcal{P}_{M_e}} \approx \mathbf{0}, \quad \frac{\partial \mathcal{F}_E}{\partial \mathcal{P}_{M_v}} = \frac{\partial \mathcal{F}_E}{\partial \mathcal{P}_{M_a}} = \frac{\partial \mathcal{F}_E}{\partial \mathcal{P}_{M_c}} \approx \mathbf{0}. \quad (5)$$

Additionally, flying at dynamic pressures q_∞ far below the one that cause the aeroelastic divergence, the “aerodynamic stiffness” associated with elastic degrees of freedom, is negligible if compared to the structural stiffness matrix \mathbf{K} . In fact, the Jacobian matrix for the elastic mode amplitudes can be approximated as a constant matrix equal to

$$\frac{\partial \mathcal{F}_E}{\partial \mathcal{P}_{M_E}} = \mathbf{K} - q_\infty \frac{\partial \mathbf{f}_a^E}{\partial \mathcal{P}_{M_E}} \approx \mathbf{K}. \quad (6)$$

The numerical computation of the terms of the Jacobian matrix associated with the flight mechanics and control degrees of freedom can be avoided if a matrix-free Generalized Minimal Residual (GMRES) Newton-Krylov subspace method²⁶ is applied only to the solution of the \mathcal{F}_R sub-system as proposed in.²⁷ Another technique relies in extracting the sensitivities using a discrete adjoint method as outlined in.²⁸

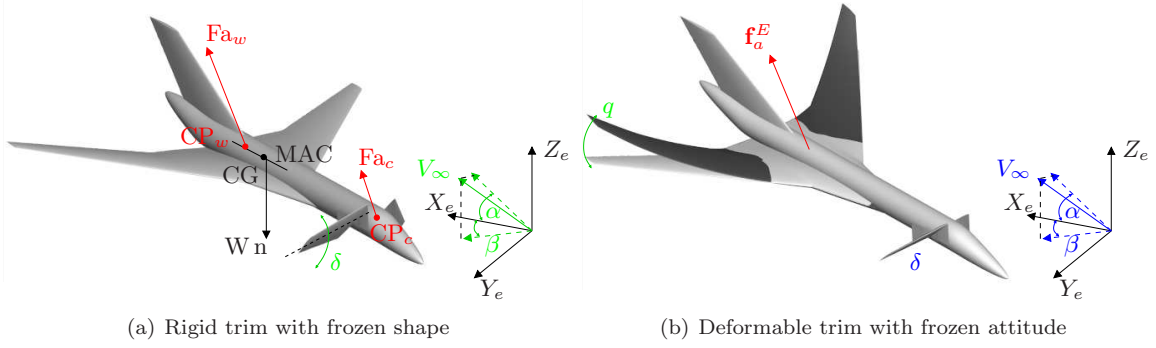


Figure 6: Staggered aeroelastic trim process.

The strategy adopted here is sketched in Fig.6(b) and can be summarized as follows. Following a sort of Gauss-Seidel solution to Eq. (1), two successive sub-problems are iteratively carried out.

A first serie of iterations are restricted to the flight mechanics equations \mathcal{F}_R , freezing the aircraft shape and changing only the \mathcal{P}_{M_v} , \mathcal{P}_{M_a} , \mathcal{P}_{M_c} parameters of the consistent problem. In this case, only the evaluation of the effect of control surface deflections \mathcal{P}_{M_c} would require a change in the computational mesh of the CFD solver. Mesh deformation procedures for such problems are rather troublesome, as outlined in.²⁹ In this case the transpiration boundary condition easily allows to consider small deflection for the control surfaces. The parameters \mathcal{P}_{M_v} are instead considered as proper boundary conditions by the CFD solver, i.e. by modifying the free-stream velocity inclination and/or using a rotating reference frame of reference. The variables controlled in the process are reported in Fig.6(a) in green colour, while those directly affected are reported in red, i.e. lifting surfaces aerodynamic forces F_a .

After the solution of the nonlinear \mathcal{F}_R , the elastic solution is determined; again, transpiration boundary condition is used to introduce the effects of the new deformed boundaries within the CFD domain. The second iterative process is carried out to find the deformed structural shape, considering here the new flight condition determined in the previous step as fixed. Again, the variables controlled in the process are reported in Fig.6(b) in green colour, while those directly affected, i.e. the generalized forces f_a^E , are reported in red. Finally, the parameters in blue are kept fixed during the iterations. In most cases, inertial accelerations are given as input, which means the trim process seeks for the flight attitude and control deflections which guarantee the equilibrium with the total amount of inertial forces, including the aeroelastic effects on the deformed shape. Despite the two systems of equations are inertially decoupled, the coupling implicitly appers through the right hand side of the system of equations.

All the aforementioned steps are repeated until convergence is reached, resulting in a trimmed deformed aircraft respecting the consistent maneuver specified by the designer. A dummy elevator mode is created, i.e. an artificial mode with unitary rigid elevator rotation keeping the rest of the aircraft as fixed. Structural displacements and elevator deflection are then accounted for in the same manner through the transpiration boundary condition. In other cases, such as the simulation of unsteady maneuvered flight, a combination of transpiration, deforming and moving meshes can be adopted, as presented in.³⁰ More in detail and considering a simple case of symmetric cruise condition, the $i - th$ iteration on the structural problem for the $n - th$ solution of \mathcal{F}_R , reads:

$$\mathbf{K}\mathbf{q}^{(i+1)} = \mathbf{f}_a^E(\mathbf{q}^{(i+1)}, \mathcal{P}_{M_v}^{(n)}, \mathcal{P}_{M_a}^{(n)}, \mathcal{P}_{M_c}^{(n)}) \quad (7)$$

A fixed-point iterative process is carried out until an equilibrium point between elastic and aerodynamic forces dependent on the assumed structural configuration is found. To avoid excessive overshoots, a relaxation

parameter $0 < \gamma < 1$ is usually introduced, i.e.:

$$\mathbf{q}^{(i+1)} = (1 - \gamma) \mathbf{q}^{(i)} + \gamma \mathbf{q}^{(i+1)} \quad (8)$$

The *inertial-relief* effect is implicitly included when generalized aerodynamic forced are determined, being the vibration modes Ψ mean axes shapes. As previously introduced, following the approach given in Eq. (7), the Jacobian of the generalized aerodynamic forces $\mathbf{K}^a = \frac{\partial \mathbf{f}_a^E}{\partial \mathcal{P}_{M_E}}$ (usually referred as aerodynamic stiffness matrix) with respect to elastic coordinates is not required, implicitly assuming the structural configuration is not in a static aeroelastic divergence condition, i.e. $\det(\mathbf{K} - \mathbf{K}^a) \neq 0$, and these terms are *small* when compared to the stiffness matrix \mathbf{K} .

Once a convergence on the deformed shape is reached, a maneuver trim loop adjusts controls and aircraft attitude to have the static equilibrium position. For simple cases, a modified Newton-Raphson iteration can be carried out once a knowledge of the linearisation of aerodynamic forces is available. These values may be known experimentally or through the CFD solver itself for example. Being aerodynamic loads non-linear, a sampling campaign to determine a database for each configuration point is required, usually based on computationally expensive finite-differences. Including aeroelastic effects on these derivatives using the CFD solver leads to further computational costs. Thus for this simple application, the term \mathbf{J}_m is never updated and determined once for all starting from the undeformed reference condition of null pitch and elevator deflection. Of course, this results in a slower convergence for trim corrections. Nevertheless the approximation introduced is motivated by the hypothesis of small structural deflections and a good guess starting point. In other cases, the Jacobian may be provided by lower-fidelity methods, e.g. panel methods, as proposed in.³¹ Of course in this case, the terms $\frac{\partial \mathcal{F}_R}{\partial \mathcal{P}_{M_e}}$ can be used, i.e. the aerodynamic derivatives including aeroelastic effects are used as done in.³²

VII. Application of NeoCASS to the Transonic CruiseR (TCR): A Case Study

The whole procedure here presented has been applied to the conceptual design of a target aircraft named TransCruiseR (TCR), most of the work packages in the SimSAC project are focusing in as test-case (depicted in Fig. 8). The TCR is meant indeed to show the difficulties in using handbook methodology when designing aircraft in the transonic speed region. In particular the goal is to compare the results gained by means of classic methodologies and the new tools such as NeoCASS developed during the project once the design specifications are given as briefly outlined in Fig. 7 and Tab. 1.

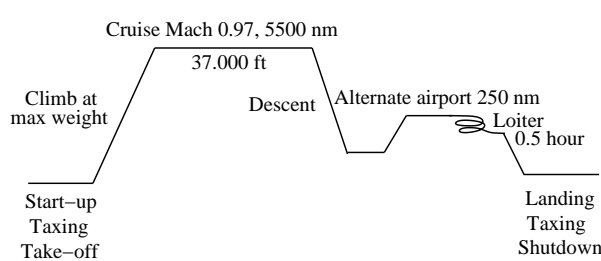


Figure 7: Mission profile for TCR

Cruise Mach	0.97 at altitude ≥ 37.000 ft
Range	5.500 nm + 250 nm to alternate airport + 0.5 hour loiter at 1.500 ft
Max payload	22.000 Kg
Passengers	200
Crew	2 pilots, 6 cabin attendants
Take-off distance	2.700 m at max W_{TO} altitude 2.000 ft
Landing distance	2.000 m at max W_L altitude 2.000 ft max payload and normal reserves
Powerplant	2 turbofans
Certification	JAR25
Maneuvering load factors	2.5, -1
Max load factors	3.1, -1.7

Table 1: Design specifications for TCR

VII.A. Geometry Description

Geometry model is defined using AcBuilder module, that allows the user to visualize all the informations, not only about geometry (Fig. 8(a)), but even about fuel distribution (Fig. 8(b)), baggage and passengers positions (Fig. 8(c)) and structural spars location Fig. 8(d).

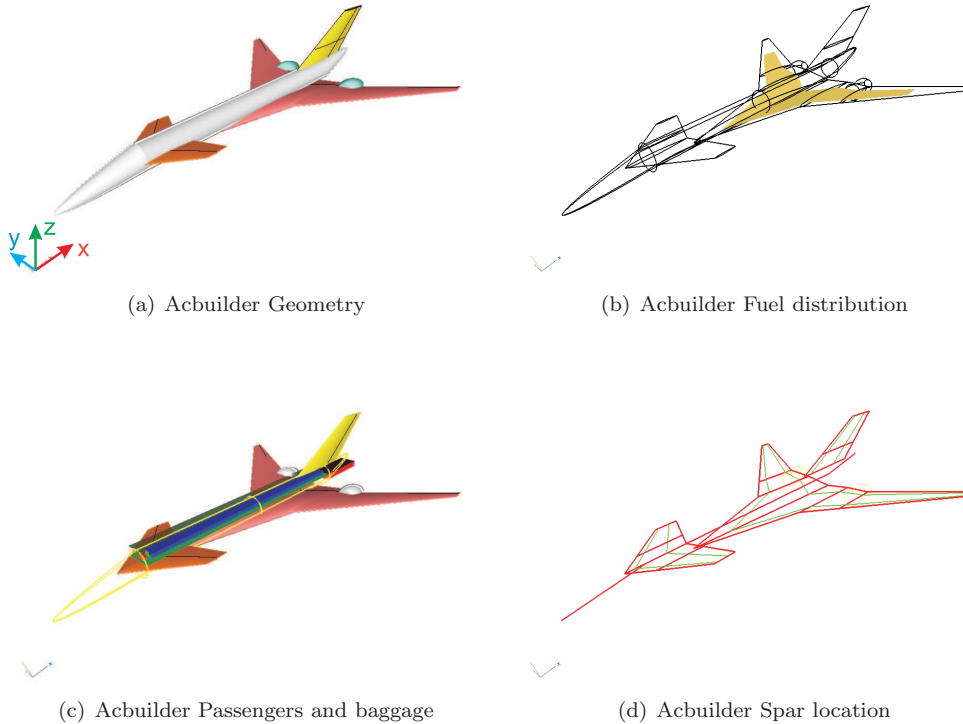


Figure 8: Acbuilder's screenshots.

Wing is described using three trapezoidal blocks, and all informations are reported in Tab. 1(a), while canard and fin are defined using two trapezoidal block and dimensions are presented in Tab. 2(a) and Tab. 2(b). Fuselage is described using a cone block for the nose, two cylindric blocks (first with linear changing diameter and second with constant diameter) and with a cone block for the tail. All data are reported in Tab. 2(b) where the inclination on nose and tail are referred to mean line of fuselage.

In table 4 are reported the Apex positions (on symmetric plane) of all aerodynamic surfaces with respect to the nose of fuselage, for x distance, and to the axes of fuselage for y and z distances, referring to the system of figure 8(a). To completely define aerodynamic geometry, data about control surface are needed. On wing there are three movable surface two independent flaps, covering the 20% of local chord, on first and second trapezoidal block, and one aileron on the final part of the last block starting in $y = 15$ m and covering the 25% of local chord. The main control surface for pitch control is represented by the canard that is all movable and has hinge axes at 50% of local chord. On the fin is present a rudder covering all the span and the 30% of the local chord.

The fuel is distributed on fuselage and on wing tanks, up to the 70% of span and delimited by the fore spar, at the 15% of local chord, and by the aft spar at the 75% of local chord.

The fore spar of canard is at the 15% of local chord, while the aft one at the 65%. For the vertical tail, the

	In	Mid	Out	
c_1 [m]	33.52	15.28	10.03	
c_2 [m]	15.28	10.03	2.45	
b [m]	4.36	4.14	13.82	
λ_{LE} [deg]	76	50	50	
Λ [deg]	3	3	3	
α_1 [deg]	1	1	1	
α_2 [deg]	1	1	-1	

	Nose	Aft	Fore	Tail
d_1 [m]	0	3.7	3.7	3.7
d_2 [m]	3.7	3.7	3.7	0
l [m]	10	20	20	10
ω [deg]	30	0	0	-15

Table 2: Wing and fuselage geometry data

	In	Out	
c_1 [m]	7	6.77	
c_2 [m]	6.77	3.43	
b [m]	2.1	3.9	
λ_{LE} [deg]	53	53	
Λ [deg]	0	0	
α_1 [deg]	0	0	
α_2 [deg]	0	0	

	In	Out	
c_1 [m]	13.96	11.51	
c_2 [m]	11.51	6.98	
b [m]	2.86	5.32	
λ_{LE} [deg]	62.03	62.03	
Λ [deg]	0	0	
α_1 [deg]	0	0	
α_2 [deg]	0	0	

Table 3: Canard and fin's geometry data.

	x [m]	y [m]	z [m]
Wing	16.8	0	-1.258
Canard	7.2	0	0
Fin	41.46	0	1.85

Table 4: Aerodynamic surface positions.

fore spar is at the 15% of local chord, while the aft at the 70%.

Finally to conclude this brief geometry description, two informations about pay load. The TCR's configuration analyzed accommodates two hundred passengers along the all length of cylindric part of fuselage, and baggage are located in the tail cone.

VII.B. Weight and Balance Results

The W&B module is used for the TCR jet transport introduced above, given its layout and its design specifications in terms of maximum payload.

Component	Mass [kg]
Wing	23.764
Canard	764
Vertical tail	955
Landing gear	6.352
Fuselage	18.623

Table 5: TCR weight survey.

Starting from an estimation of a total fuel amount of 106.186 kg , distributed between integrated wing tanks and fuselage central tank, the predicted MTOW is 193.672 kg , while the MEW is 69.093 kg. A brief survey of the main weights of different components is reported in Tab. 5. The values reported represent only the structural contribution which is the focus of the present work. Again, non-structural masses, such as systems, furniture and interior, are estimated separately if not directly given by the user and contribute to the total weight of each component; for example the actual fuselage mass is the sum of the value reported in the table and 17.966 kg due statistically estimated furniture and interior.

Finally, the estimated positions of the center of gravity along the longitudinal axis for the two configurations (the length of the fuselage is 60 m) together with the principal moment of inertia estimated by statistical formulas at MTOW are reported in table 6.

x_{MEW} [m]	x_{MTOW} [m]	I_{xx} [kgm^2]	I_{yy} [kgm^2]	I_{zz} [kgm^2]
36,55	36,6	$9,502 \cdot 10^6$	$2,015 \cdot 10^7$	$2,7737 \cdot 10^7$

Table 6: TCR inertia survey.

These values will be then used in the structural sizing process for the determination of inertial loads and finally compared to the new predicted values which consider the real load bearing material distribution.

VII.C. First Structural Sizing Results Obtained Using GUESS

Structural sizing was derived using the two strategies available in GUESS, *standard mode* and *modify mode*. The first one uses loads due to prescribed maneuvers, solved using regulation (like yawing maneuver conditions due to one engine out) or considering the aircraft as a point mass located into its CoG and subject to resulting inertial and aerodynamic loads (like ones due to a pull-up maneuver at a prescribed load factor).

	x_{MTOW} [m]	I_{xx} [kgm^2]	I_{yy} [kgm^2]	I_{zz} [kgm^2]
W&B	36.6	$9,502 \cdot 10^6$	$2,015 \cdot 10^7$	$2,7737 \cdot 10^7$
GUESS standard mode	35,22	$5,5465 \cdot 10^6$	$1,8205 \cdot 10^7$	$2,3034 \cdot 10^7$
GUESS modified mode	35,72	$5,4776 \cdot 10^6$	$1,8224 \cdot 10^7$	$2,2691 \cdot 10^7$

Table 7: TCR weight and inertia survey.

The second one couples the GUESS's sizing routines with the SMARTCAD's rigid trim solver. The user defines a set of frozen maneuvers that will be used to compute the sizing load distributions. GUESS generates the first aeroelastic model using the standard mode, then sizes the structure using the trim's solutions, by updating, at each step, the inertial property of beam elements.

The following three frozen maneuvers are considered to size the aircraft using modify GUESS:

1. Normal load factor $n_z = 3.1$, $z = 0$ m, $M_\infty = 0.6$,
2. Cruise flight with sideslip angle $\beta = 25$ deg, $z = 0$ m, $M_\infty = 0.65$,
3. A transition from levelled flight into a snap-roll given abrupt deflection on the canard and the rudder, $z = 0$ m, $M_\infty = 0.6$, $\delta_c = 30$ deg, $\delta_r = 30$ deg.

After the structural sizing, the new MTOW weight for the TCR is equal to 215.211 kg for GUESS standard mode and 223.679 kg for the modify mode. These weights are determined considering two regressions on load-bearing material which is numerically determined for the considered aircraft under physical basis. Furthermore, the position of the center of gravity for the MTOW configuration and total inertias are reported in Tab. 7 for both methods and compared with the previous estimations of W&B. Table 8 compares the results by W&B with the new estimation of the structural components determined by GUESS, both in standard and modify modes: both the weight of the load-bearing material and the two steps of regression to account for secondary airframe components are reported. As it is possible see, the results obtained with modify mode and standard mode are very different each other, especially concerning the vertical tail and the canard, and both result sets are very different from the values predicted by W&B. It is interesting to compare the structural mass distribution on the four components (wing Fig. 9(a), fuselage Fig. 9(b), canard Fig. 9(c), vertical tail Fig. 9(d)) obtained with the two methods. The wing mass distribution is quite similar, while the others are not. The fuselage obtained using standard mode has a maximum, at the wing position, lower than that obtained with modify mode, while presents another local maximum, at the canard position, bigger than obtained with modify mode. Also observing the canard mass distribution, it is easy to understand that standard mode, due to particular geometry and hight sweep angle of wing, does not share loads well on wing and canard, and therefore on fuselage.

Concerning the vertical tail, it is possible to say that in this case the yawing maneuver conditions regulations are not sufficient to size the fin.

Component	GUESS [kg] bearing material		GUESS [kg] primary weight		GUESS [kg] total		W&B [kg]
	S.M.	M.M.	S.M.	M.M.	S.M.	M.M.	
Wing	15.506	19.353	21.176	26.429	27.367	34.156	23.764
Canard	2.373	899	3.240	1.228	4.188	1.587	764
Vertical tail	2.268	4.756	3.097	6.496	4.003	8.395	955
Fuselage	9.060	10.849	12.663	15.162	17.235	20.637	18.623

Table 8: TCR weight survey

The main difficulty in this phase is the creation of a stick model which can also faithfully represent the assumed mass distribution of the payload and non-structural mass. Representing concentrated items like engines, auxiliary tanks and landing gears by means of lumped masses rigidly attached to the main structure is trivial. Introducing distributed masses like the fuel in the wing-box, paint, passengers, furniture and especially the secondary structural weight which is only predicted as a value by the regression curve, is more complicated. Therefore, two solutions are here adopted:

- secondary structural masses are simply placed as lumped masses on the nodes of the mesh proportionally to the volume of the beams;
- payload is considered as non-structural mass per unit length using the same approach previously mentioned

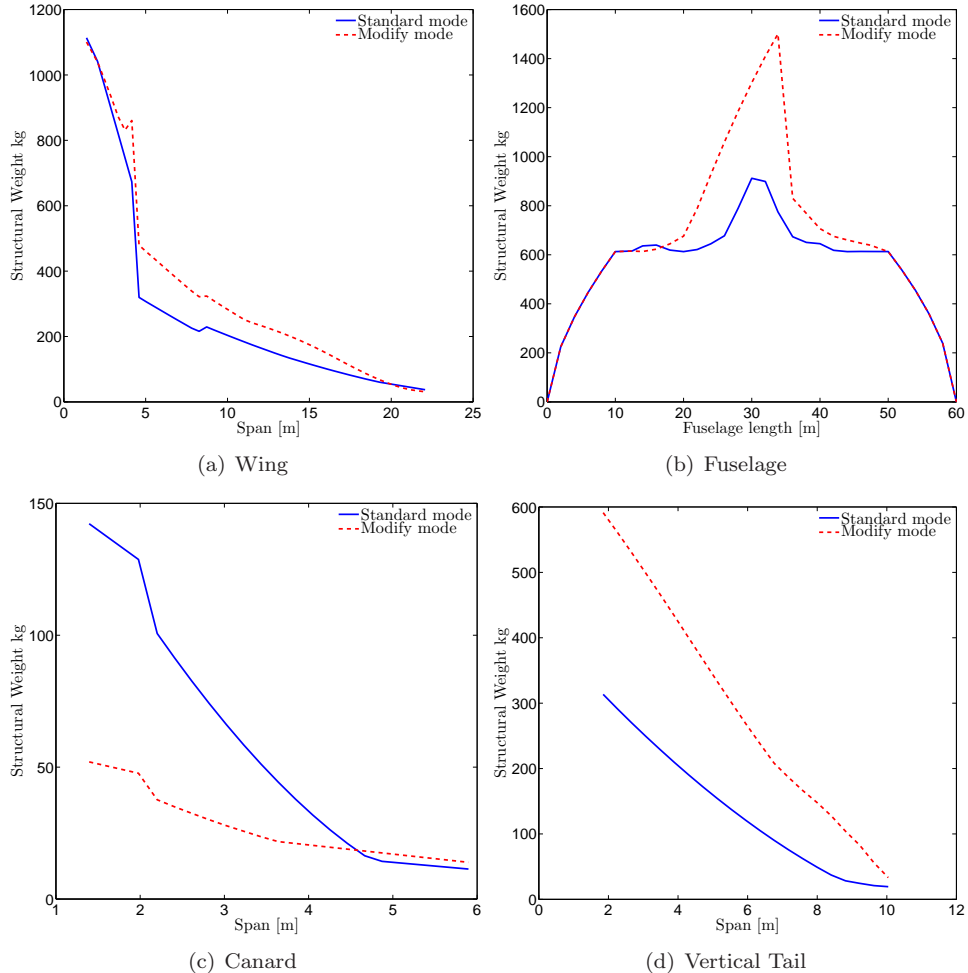


Figure 9: Mass distribution

Besides these assumptions, the reader is warned usually a simple model with fewest degrees of freedom as possible is desired for fast aeroelastic evaluations; this may introduce further approximations in the discretization of the distributed masses due to the coarseness of the model. Fig. 10 gives an overview of the aero-structural mesh created for the aeroelastic and MDO procedures. Since GUESS has a complete knowledge of the parameters which rule the geometry of the aircraft, it is also possible to create the Vortex/Doublet Lattice mesh. Also, GUESS automatically creates stress-recovery points on the boundary limits of every beam (along lifting surfaces wing-box or fuselage diameter) and transfers to SMARTCAD all its database in terms of material and beam properties, nodes, connectivities, aerodynamic mesh and control surfaces position. The structural model chosen to conduct all the following analysis is that obtained using GUESS in modify mode. This model has been validated comparing the inertial properties and the modal solution obtained using both NeoCASS and MSC/NASTRAN. The latter model was defined automatically starting from NeoCASS model thanks to an ad hoc script specifically developed for this aim.

In table Tab. 9 is reported a comparison about the first twelve frequencies and in Tab. 10 about inertial properties. Observing the results, it is possible to say that there is a very good correlation between the two structural models.

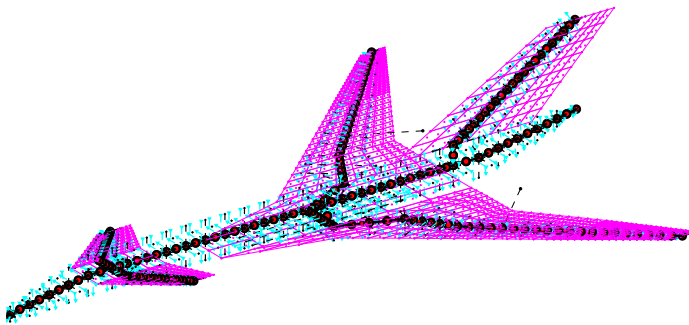


Figure 10: Aero-structural mesh

	m 7	m 8	m 9	m 10	m 11	m 12	m 13	m 14	m 15	m 16	m. 17	m 18
NeoCASS	1.85	2.27	2.48	2.69	2.92	3.36	4.18	5.00	5.73	6.44	6.98	8.41
MSC/NASTRAN	1.84	2.28	2.49	2.71	2.94	3.35	4.12	5.03	5.78	6.48	6.94	8.36

Table 9: First twelve frequencies

VII.D. Aeroelastic Analysis Using SMARTCAD: Frozen Maneuvers

The methodology adopted in SMARTCAD is the classic approach used in linear aeroelastic analysis³³ which allows to perform rapid trim calculations for the restrained/unrestrained aircraft and evaluate the corrections to its stability derivatives due to the structural flexibility. At this early phase, we start investigating the quality of the preliminary sizing especially considering its integrity and the requirements on the maximum displacements and deflections allowed. The methodology developed enables the user to compare the solution of the trim to the rigid case and to evaluate any lack in terms of control deflections required to perform the maneuver and excessive stability derivatives changes due to deformability. For the test-case here considered, the following frozen maneuvers are considered in order to overweight some lacking points in the initial sizing process done using GUESS:

1. normal load factor $n_z = 3.1$, $z = 5000$, $M_\infty = 0.6$;
2. a high-speed steady rolling pullout given an aileron input δ_a of 25 degrees, vertical load factor of $n_z = 3.1$ (and corresponding pitch rate $q = (-n_z - 1) g/V_\infty$), $z = 5000$ m, $M_\infty = 0.6$.
3. cruise flight with sideslip angle $\beta = 20$ deg, $z = 5000$ m, $M_\infty = 0.6$ and $z = 10000$ m, $M_\infty = 0.9$;
4. a transition from levelled flight into a snap-roll given an abrupt deflection of the elevator and the rudder, $z = 5000$ m, $M_\infty = 0.6$ and $z = 1000$ m;
5. an abrupt aileron input δ_a of 25 degrees starting from cruise flight, $z = 5000$ m, $M_\infty = 0.6$;

	x_{MTOW} [m]	MTOW [kg]	I_{xx} [kgm^2]	I_{yy} [kgm^2]	I_{zz} [kgm^2]
Neocass	35,72	223.679	$5,4776 \cdot 10^6$	$1,8224 \cdot 10^7$	$2,2691 \cdot 10^7$
MSC/NASTRAN	35,71	223.819	$5,2862 \cdot 10^6$	$1,8006 \cdot 10^7$	$2,2729 \cdot 10^7$

Table 10: Weight and inertia comparison

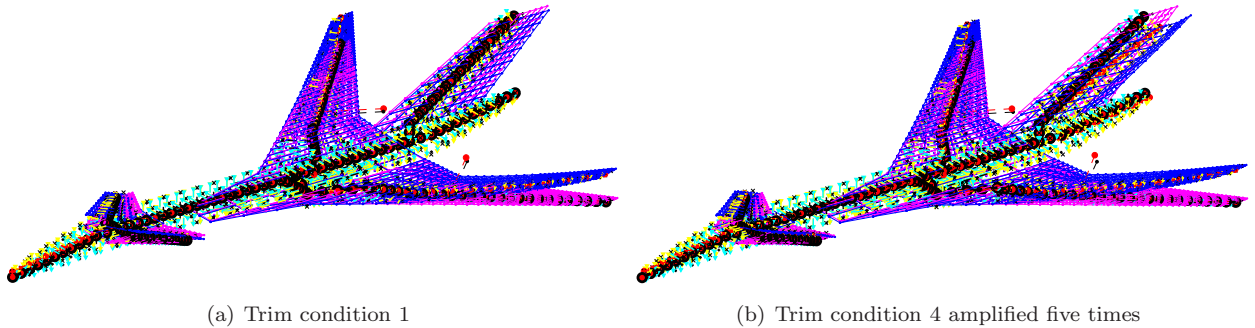


Figure 11: Deformed model, load condition 1

The conditions proposed, should represent a good load-set for the airframe for fuselage, wing, canard and fin. The maneuvers 1-2 and 3-4 give rise to the worst load conditions for wing-canard-fuselage and fin, respectively. Stresses on wing sized using GUESS in standard mode exceed the maximum allowed value, while this does not happen in the case of the structure obtained using GUESS in modify mode, and the same happens in the case of fuselage. On the contrary, it is possible to see that GUESS in standard mode oversizes the structure. Finally, the load conditions considered by GUESS standard mode are not enough to correctly size the fin structure.

VII.E. Rigid vs. Deformable Stability Derivatives

As already described in the previous paragraphs, the approach adopted for the static aeroelasticity makes very easy the calculation of the so called deformable stability derivatives, that include the effect of structural deformability and represent a good indication about the reliability of the structural design.

In Tables 11 and 12 a comparison between Rigid and Deformable stability and control derivatives, computed at Mach number $M = 0.6$, obtained using the two structural models generated by GUESS in standard and modify modes, is reported.

VIII. SMARTCAD Validation Using Low, Medium Fidelity CFD-based Tools and Wind Tunnel Testing

In this section, low and medium fidelity methods are applied to the TCR in order to validate the overall analysis tool and to evaluate the enhancements provided by the latter. In this respect, few aspects will be covered: aerodynamic load predictions, trim analysis for the rigid and deformable cases and aerodynamic derivatives evaluation and correction for aeroelastic effects. Regarding the low fidelity tool used for SMARTCAD result validation, MSC/NASTRAN has been adopted, since it represents a standard 'de facto' for the aerospace industry. Concerning the medium fidelity tool based on the CFD, the code Edge by FOI has been selected.

The adoption of CFD model is justified by the need of resulting in enhanced flow predictions compared to the classic linear theories. On the other hand, CFD models are computationally demanding and need particular techniques when aeroelastic analysis has to be carried out. Thus, special care has to be taken to reduce the costs and raise the robustness of the algorithms so that this technology can be automatically included in the early design process.

In this work, Euler equations are considered as a good compromise for enhanced flow modelling, mesh requirements and hence costs. They allow to include compressibility effects in the analysis and require for coarser meshes and fewer restrictions than for Navier-Stokes simulations. Also, automatic mesh generation for unstructured meshes can be exploited, once a water-tight CAD file is given, allowing to recursively have

(a) α derivatives						
	Rigid		Deformable		Deformable/Rigid	
	Standard	Modified	Standard	Modified	Standard	Modified
C_{L_α}	3.72	3.72	2.86	3.11	0.77	0.84
C_{M_α}	-0.69	-0.69	0.06	-0.22	-0.09	0.31

(b) β derivatives						
	Rigid		Deformable		D/R	
	Standard	Modified	Standard	Modified	Standard	Modified
C_{S_β}	0.29	0.29	0.26	0.28	0.88	0.94
C_{L_β}	-0.13	-0.13	-0.16	-0.14	1.19	1.05
C_{N_β}	0.13	0.13	0.11	0.12	0.87	0.93

(c) p derivatives						
	Rigid		Deformable		D/R	
	Standard	Modified	Standard	Modified	Standard	Modified
C_{S_p}	0.03	0.03	0.04	0.04	1.46	1.53
C_{L_p}	-0.49	-0.49	-0.41	-0.43	0.84	0.88
C_{N_p}	-0.01	-0.01	-0.00	-0.00	0.40	0.40

(d) q derivatives						
	Rigid		Deformable		D/R	
	Standard	Modified	Standard	Modified	Standard	Modified
C_{L_q}	6.34	6.34	4.81	5.17	0.76	0.82
C_{M_q}	-6.79	-6.79	-5.47	-5.88	0.81	0.87

(e) r derivatives						
	Rigid		Deformable		D/R	
	Standard	Modified	Standard	Modified	Standard	Modified
C_{S_r}	-0.37	-0.37	-0.31	-0.34	0.84	0.92
C_{L_r}	0.17	0.17	0.17	0.17	1.00	0.96
C_{N_r}	-0.17	-0.17	-0.14	-0.16	0.84	0.92

Table 11: Stability Derivatives $M = 0.6$

(a) $\delta_{aileron}$ derivatives						
	Rigid		Deformable		D/R	
	Standard	Modified	Standard	Modified	Standard	Modified
$C_{S_{\delta_a}}$	-0.01	-0.01	-0.01	-0.01	1.37	1.55
$C_{L_{\delta_a}}$	0.10	0.10	0.02	0.06	0.16	0.56
$C_{N_{\delta_a}}$	-0.00	-0.00	-0.01	-0.01	1.46	1.48

(b) δ_{rudder} derivatives						
	Rigid		Deformable		D/R	
	Standard	Modified	Standard	Modified	Standard	Modified
$C_{S_{\delta_r}}$	-0.13	-0.13	-0.09	-0.11	0.68	0.83
$C_{L_{\delta_r}}$	0.02	0.02	0.02	0.02	1.19	1.10
$C_{N_{\delta_r}}$	-0.07	-0.07	-0.05	-0.06	0.71	0.85

(c) δ_{canard} derivatives						
	Rigid		Deformable		D/R	
	Standard	Modified	Standard	Modified	Standard	Modified
$C_{L_{\delta_c}}$	0.05	0.05	0.00	0.00	0.05	0.04
$C_{M_{\delta_c}}$	0.30	0.30	0.34	0.32	1.13	1.05

Table 12: Control Derivatives $M = 0.6$

a new mesh when the external shape of the aircraft is changed.

When aeroelastic analysis based on CFD models is considered, the complexity is further raised. The flow domain has to be updated to follow the new deformed shape of the aircraft. This demands for special techniques which are both computationally demanding and sometimes lack of sufficient robustness. In this case, this issue is overcome in the within the medium fidelity approach in favour of the transpiration method.³⁴ For inviscid cases and when the structural motion is relatively small, i.e. within the usual linear elastic behavior, the domain need not to be updated; the structural effects are simply accounted for as a change in the boundary condition along the walls. This also eases the management of control surfaces deflection which are required when the trim condition for a free flying aircraft has to be sought. For the classic linear aeroelastic analysis, the solution is recovered by a matrix of Aerodynamic Influence Coefficients (AIC) ruling the relation between the aerodynamic loads and the structural deformation. When non-linear CFD methods are adopted, this is troublesome and an iterative process is required. The approach adopted here follows the one proposed in Section VI: a staggered iterative process is carried out which at first determine the flight parameters, e.g. angle of attack and control deflections, to have the aircraft trimmed with a given deformed shape; on a second stage, the new deformed shape is sought with frozen flight parameters by solving the structural equations. The process is iterated until overall convergence is gained. For simple cases, the aerodynamic derivatives with respect to flight parameters can be efficiently used as pursued here.

Data transfer between the aerodynamic mesh and the structural has to be carried out, so that data, e.g. displacements velocities or forces, are transferred among the common boundaries. This is a well-known issue in aeroelasticity, not only when CFD methods are adopted. In the present work, two methods available in SMARTCAD are used to transfer data with the CFD flow solver: the Moving Least Squares (MLS) technique¹⁸ or Radial Basis Function (RBF) interpolation is used.¹⁹

Keeping in mind the need to reduce computational costs, a modal approach has been adopted together with the creation of Reduced Order Models which allow to extract important pieces of information regarding the flow system with few simulations. ROMs can be used to determine the steady and dynamic aerodynamic

derivatives of the aircraft and easily correct them for the aeroelastic effects. Furthermore, they can be used for a rapid flutter assessment.³⁵

Finally, the comparison between numerical and experimental stability derivatives for the rigid aircraft is also reported. Indeed, during SimSAC project a 1:40 scale model was designed and manufactured by Politecnico di Milano and tested for steady and unsteady stability derivatives measurement by TsAGI (see Fig. 12).

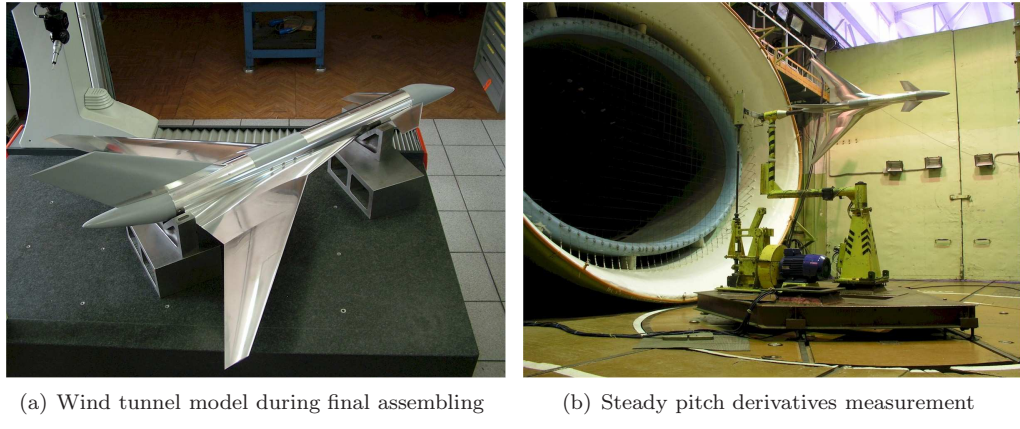


Figure 12: TCR wind tunnel model.

VIII.A. CFD Aerodynamic Model and Comparisons

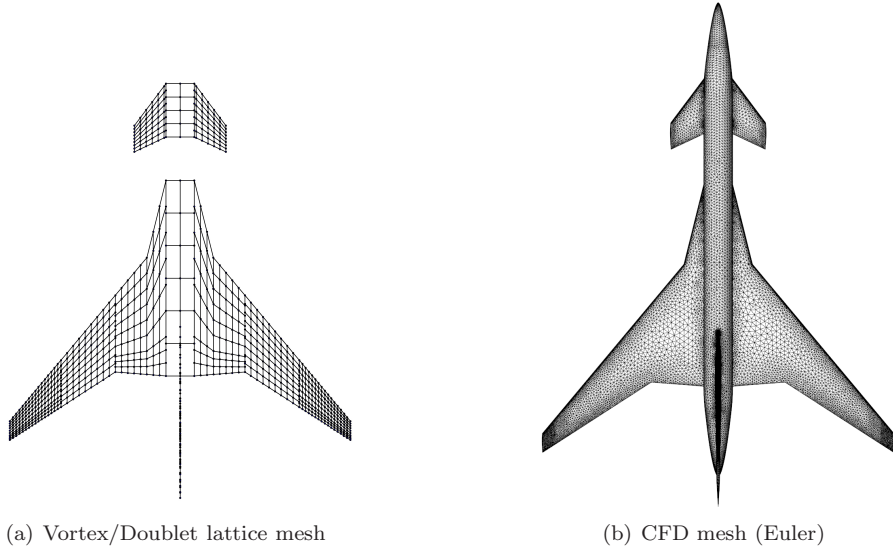


Figure 13: Meshes adopted in low and medium fidelity analysis (top view).

Figure 13 depicts the two aerodynamic meshes adopted for low and medium fidelity analysis in the present work. The main difference relies in how the geometry of the fuselage and its intersection with the lifting surfaces is accounted for. In this case, the VLM/DLM mesh represents the fuselage as a simple distribution of flat panels in the plane of the wings only. This allows to maintain the continuity of the aerodynamic load at the root of the lifting surfaces. No longitudinal modelling has been considered, i.e. the vertical

tail has no intersection with the fuselage with all boundaries as free. However, in the present work only symmetric flight conditions have been considered which make this detail of minor importance with respect to the overall quality of the results. Table 13 reports few details about the two meshes. The VLM/DLM mesh is represented by 18 patches with a total number of 787 panels. The CFD mesh used for inviscid analysis features 178.158 volume elements and 70.432 surface elements along the aircraft surface. Despite the latter is not so fine for common CFD application, the differences with the former in terms of surface discretization and in geometric detail modelling are evident. In order to neglect compressibility and viscous

Component	VLM/DLM panels	CFD points
Wing	594	45.565
Canard	96	10.335
Fin	77	6.526
Fuselage	20	8.006

Table 13: Distribution of panels for the DLM/VLM and CFD meshes.

effects, a subsonic case at flight Mach number $M_\infty = 0.65$ and null incidence has been considered, resulting a consistent and fair comparison for the different models.

Table 14 reports the values of the reference normal force coefficient CN_0 and of the pitching moment Cm_0 with respect to the center of gravity for the CFD and the VLM models available respectively in SMARTCAD and MSC/NASTRAN. For this last, a simple flat model has been considered, i.e. no built-in effects given by twist or airfoil camber, which explains the relatively higher values of forces and moments. For the flat plate case indeed, the normal aerodynamic force is higher and leads to a higher value of the pitching moment. All

	Edge	SMARTCAD	MSC/NASTRAN
CN_0	0.14	0.17	0.24
Cm_0	-0.12	-0.09	-0.12

Table 14: Intercepts at the reference flight condition, $\alpha = 0$ deg, $M_\infty = 0.65$, $z = 0$ m.

the models predict a pitch down aerodynamic moment with the CFD solution falling between the two low fidelity predictions. Nevertheless, for this case the results can be considered as satisfactory.

The aerodynamic derivatives for the reference condition have been determined through Finite Difference (FD). For the three different models considered, Table 15 summarizes the longitudinal derivatives of the normal force and pitch moment with respect to the angle of attack α and canard deflection δ . The wind tunnel results are also reported in the last column (WT) for comparison.

	Edge (FD)	SMARTCAD	MSC/NASTRAN	WT
CN_α	3.56	3.92	3.46	3.01
Cm_α	-1.25	-0.72	-0.80	-1.00
CN_δ	0.05	0.06	0.04	0.06
Cm_δ	0.44	0.33	0.27	0.40

Table 15: Longitudinal steady derivatives, $M_\infty = 0.65$, $z = 0$ m, rigid

The larger differences between low and medium fidelity analysis come from the pitching moment derivatives, implying a different pressure load distribution and resultant. Considering the canard for example, the

CFD solution results in lower normal force derivative but higher pitching moment, highlighting the importance of local fuselage effects. For the CFD case, the same derivatives have also been determined through a ROM for the rigid body modes at low reduced frequencies for two conditions: $\alpha = 0$ and $\alpha = \alpha_T$ which is the angle of attack for the trimmed solution outlined in the next section. As shown in Tab. 16, good agreement between the FD, ROM and wind tunnel testing has been found.

Finally, dynamic derivatives for the rigid aircraft have been considered and reported in Tab. 17. The results of the ROMs by CFD and the DLM methods available in SMARTCAD and MSC/NASTRAN are compared together with wind tunnel measurements. As expected, the results provided by enhanced fidelity method are closer to the experiment. Large discrepancies have been determined for the pitching moment derivatives with $\dot{\alpha}$ and q . Again, the contribution of the fuselage is not negligible.

	Edge (FD) $\alpha = 0$	Edge (ROM) $\alpha = 0$	Edge (ROM) $\alpha = \alpha_T$	SMARTCAD	MSC/NASTRAN
CN_α	3.56	3.57	3.57	3.92	3.46
$k = 0.01$		3.55	3.56		
Cm_α	-1.25	-1.29	-1.16	-0.72	-0.80
$k = 0.01$		-1.32	-1.22		
CN_δ	0.05	0.04	0.08	0.06	0.04
Cm_δ	0.43	0.45	0.53	0.33	0.27

Table 16: Longitudinal steady derivatives, $M_\infty = 0.65$, $z = 0$ m, rigid

	Edge (ROM) $\alpha = 0$	SMARTCAD	MSC/NASTRAN	WT
$CN_{\dot{\alpha}}$	0.16	-0.63	-0.25	1.25
CN_q	-6.22	-5.70	-5.93	-6.34
$CN_{\dot{\alpha}} + CN_q$	-6.20	-6.34	-6.18	-5.09
$Cm_{\dot{\alpha}}$	19.19	0.79	1.11	19.00
Cm_q	-24.42	-6.64	-4.25	-22.81
$Cm_{\dot{\alpha}} + Cm_q$	-5.22	-5.85	-5.36	-3.67

Table 17: Longitudinal dynamic derivatives, $M_\infty = 0.65$, $z = 0$ m, rigid.

VIII.B. Trim Analysis

The trim condition for TCR case in simple symmetric cruise flight at MTOW, $M_\infty = 0.65$, $z = 0$ has been sought. As mentioned above, a subsonic flight regime has been considered in order to ease the validation process among the tools. The methods have been applied for both the rigid and deformable case. The former can be considered as a subcase of the latter, by simply switching-off the aerodynamic feedback on the structural equation in the overall equilibrium solution.

For the simple rigid case considered, the unknowns of the problem are represented by the angle of attack α and the deflection of the canard δ with a normal load factor $n_z = 1$. The results are summarized in Tab. 18 and compared with those provided by SMARTCAD and MSC/NASTRAN. The values predicted by Edge and SMARTCAD relatively agree, considering the models are quite different. A small negative value of α and a relatively high canard deflection required to balance the aircraft are predicted. This would probably

demand for improvements in the weight and balance process or in the aerodynamic layout design during the design phase. Larger discrepancies are determined by MSC/NASTRAN which neglects in this case the built-in twist effects on the reference aerodynamic loading.

	Edge	SMARTCAD	MSC/NASTRAN
α_T	-0.08	-1.57	2.37
δ_T	13.93	18.25	7.82

Table 18: Trim solution summary, $M_\infty = 0.65$, $z = 0$

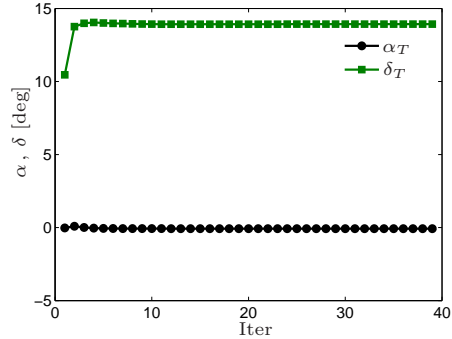


Figure 14: Solution history, $M_\infty = 0.65$, $z = 0$ m

Fig. 14 shows the history of the iterative trim process on α and δ for the CFD trim process. The initial reference condition is $\alpha = 0$ and $\delta = 0$. Being the problem basically linear, the first iteration based on the derivatives determined in corresponded of this reference condition leads immediately to a solution very close to the final result. In the following iterations indeed, only minor adjustments occur.

Mode	Freq. [Hz]	Description
7	1.85	First wing bending
9	2.48	Fuselage bending
12	3.36	In-plane wing bending
13	4.18	First torsional wing
16	6.44	Second wing bending
101	0.0	Rigid canard deflection

Table 19: Modal base adopted for the aeroelastic trim.

As for the deformable trim, the structural contribution is considered in two different ways: the full FE model is used for the low fidelity analysis with SMARTCAD while a modal approach is adopted for the CFD process. In this case, the modal base consists in the first five free-free vibration modes and the canard rigid deflection. Some of the considered modes are reported in Fig. 15 and briefly summarized in Tab. 19.

The history of the trim process is outlined in Fig. 16. After the first iterative loop on the fixed-shape trim problem, the trend is different compared to the one determined in the rigid process (see Fig. 14); the deflection of the canard is significantly affected by the effect of structural deformability on the lifting surfaces, while a relatively small increase in α is required to compensate for their washout.

The convergence on the elastic problem, a part from the first six iterations, is fairly smooth and rapid. The first two vibration modes govern the structural response; the addition of further modes in the original modal base have turned out to add for negligible contributions to the final solution. After approximately ten iterations the problem has converged.

Fig. 17 shows the difference in the pressure coefficient distribution between the reference initial condition and the final one. The major difference occurs on the canard which again undergo relatively large deflection to compensate for the pitch moment. Fig. 18 shows the difference in pressure distribution between the trim solution for the rigid and deformable case along three different spanwise sections of the canard, respectively

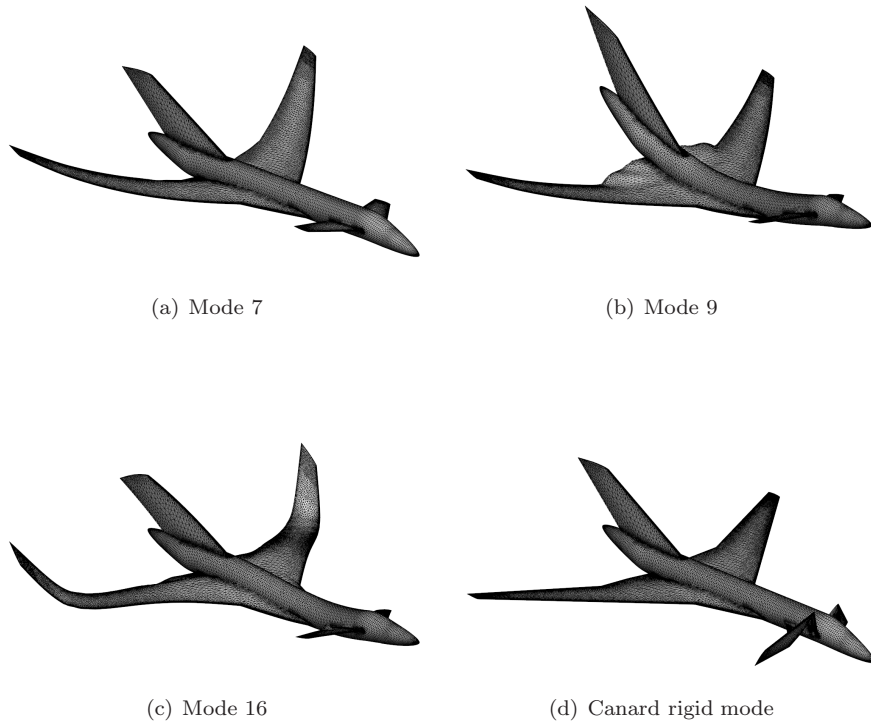


Figure 15: Example of mode shapes considered for the aeroelastic trim.

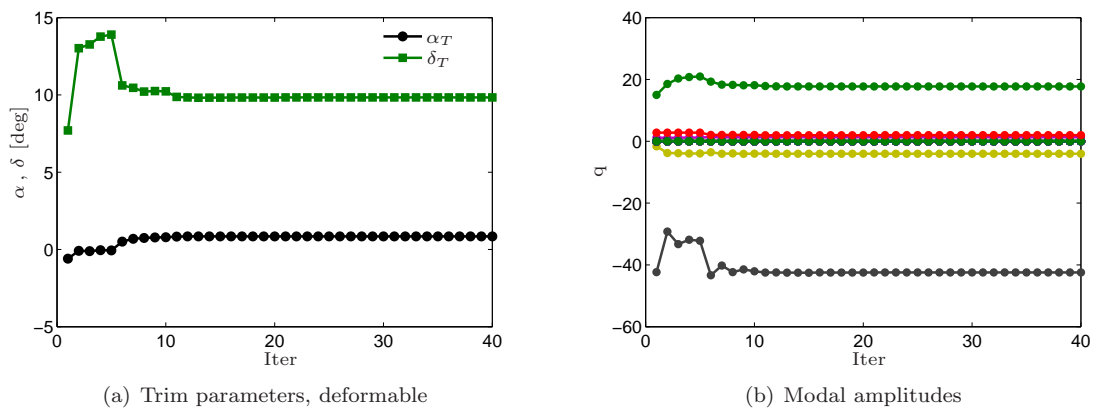


Figure 16: Trim solution, $M_\infty = 0.65$, $z = 0$ m.

	Edge	SMARTCAD	MSC/NASTRAN
α_T	0.84	-0.17	3.53
δ_T	9.84	10.38	1.34
$\Delta s_{x,wtip}$	0.01	0.03	0.02
$\Delta s_{z,wtip}$	0.94	0.73	0.97
$\Delta s_{z,ctip}$	0.12	0.14	0.08
$\Delta\theta_{x,wtip}$	0.05	0.03	0.06
$\Delta\theta_{y,wtip}$	-0.05	-0.06	-0.04
$\Delta\theta_{x,ctip}$	0.00	0.013	0.00
$\Delta\theta_{y,ctip}$	0.01	-0.00	0.00

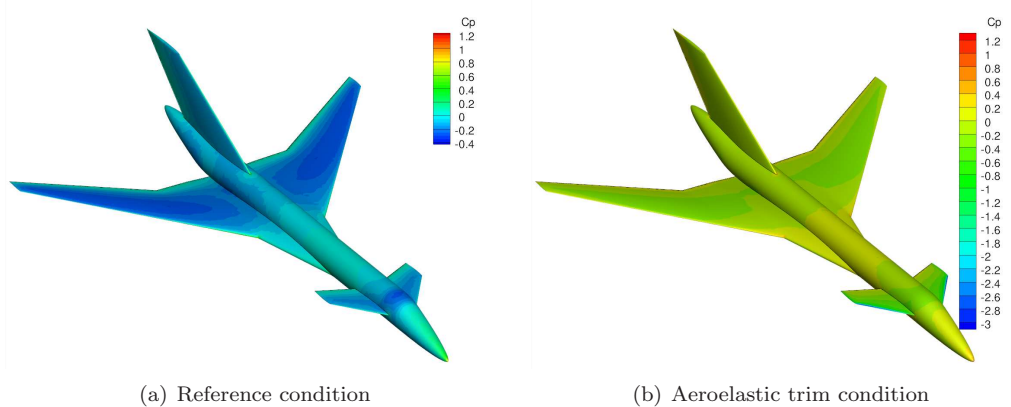
Table 20: Symmetric trim solution, $M_\infty = 0.65$, $z = 0$ m, deformable.

Figure 17: Pressure coefficient contour for the reference and final deformed trimmed condition.

at a span fraction $\eta = 0.5, 0.66$ and 0.83 . Since the deflection of the canard is lower than the rigid case, the overall aerodynamic load is reduced.

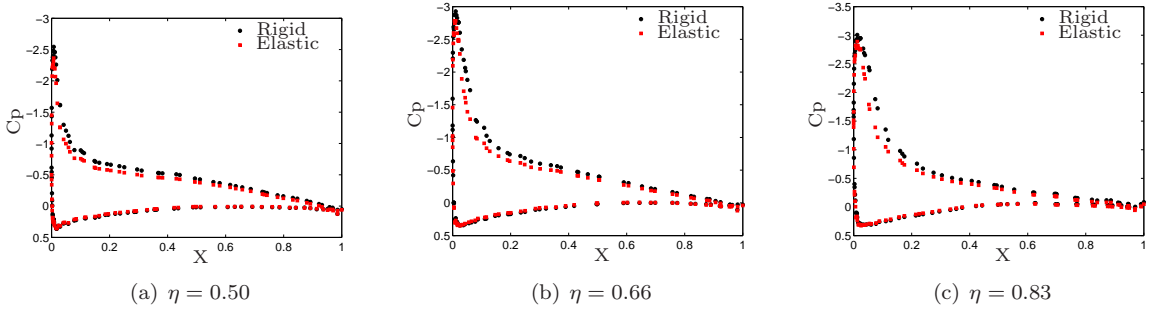


Figure 18: Canard chordwise pressure coefficient, $M_\infty = 0.65$, $z = 0$ m.

As for the wing, Fig. 19 highlights the aeroelastic effects along three different spanwise sections at $\eta = 0.44, 0.67$ and 0.89 . The re-distribution for the aerodynamic load is clear. Because of aeroelastic effects and the washout occurring especially in the outboard sections, the spanwise resultant is shifted inboard. The trim so-

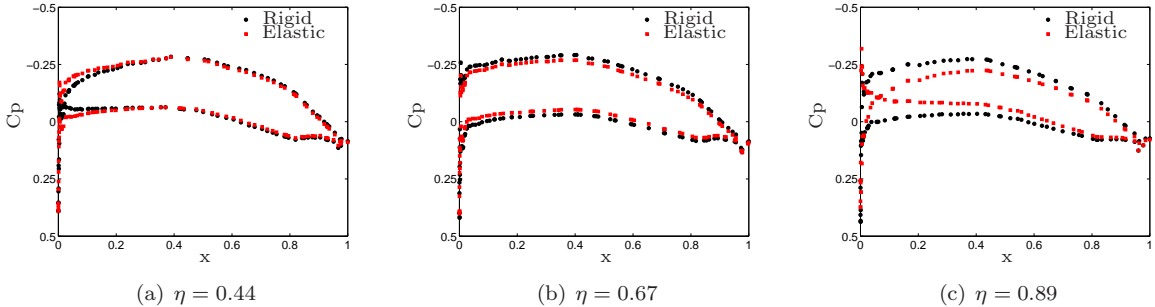


Figure 19: Wing chordwise pressure coefficient, $M_\infty = 0.65$, $z = 0$ m.

lution for the elastic aircraft is compared with the results from linear theories available in SMARTCAD and MSC/NASTRAN. As reported in Tab. 20, α has to be increased and δ decreased when deformability is accounted for. SMARTCAD and Edge have a fairly good agreement for the trim parameters, while the solution provided by MSC/NASTRAN features larger discrepancies, being affected by the reference load which does not consider camber effects. The increase in α is approximately of 1 deg for all the methods adopted; SMARTCAD shows the largest variations in both α and δ . This implies the trimmed solution determined by SMARTCAD features higher differences in the re-distribution of the aerodynamic load compared to the rigid case. Such differences can be better highlighted considering the final deformed shape, briefly summarized in Tab. 20 in terms of the relative displacement Δs and deflection $\Delta\theta$ between the tip and the supported nodes.

Considering again the solution provided by SMARTCAD, the wing tip features the lowest vertical displacement and highest twist deflection (the negative sign means here the local angle of attack is reduced). Thus, the aerodynamic resultant for the wing is moved inboard and hence upstream, implying a higher reduction in the canard deflection compared to the rigid case. As for the canard, no appreciable difference is highlighted.

VIII.B.1. Aeroelastic Derivatives

In terms of aerodynamic derivatives, Tab. 21 reports the values for the longitudinal derivatives for the elastic aircraft at the flight condition considered, $q_\infty = 29645$ Pa. As for the solution predicted by Edge, the effects

of the reference condition about the linearization point can be also included.

	Edge (ROM) $\alpha = 0$	Edge (ROM) $\alpha = \alpha_T$	SMARTCAD	MSC/NASTRAN
\mathbf{CN}_α	2.86	2.85	2.80	2.51
$k = 0.01$	2.84	2.83		
\mathbf{Cm}_α	-0.51	-0.36	0.15	-0.05
$k = 0.01$	-0.55	-0.42		
\mathbf{CN}_δ	-0.05	-0.02	0.002	0.003
\mathbf{Cm}_δ	0.53	0.62	0.36	0.29

Table 21: Aeroelastic longitudinal steady derivatives, $M_\infty = 0.65$, $z = 0$ m, deformable.

A different ROM has been indeed determined for each condition, i.e. $\alpha = 0$ or $\alpha = \alpha_T$. Also, the value of the steady derivatives with α can also be compared for a very low value of the reduced frequency k when a plunge motion is considered for the evaluation of the derivative. The differences between the rigid and elastic cases can be better highlighted considering Tab. 22 which reports the correction coefficients η , defined as the ratio of the elastic and rigid values, i.e. $\eta(\cdot) = \frac{(\cdot)_E}{(\cdot)_R}$. All the three methods adopted lead to a good agreement for the corrections to \mathbf{CN}_α and \mathbf{Cm}_δ . This last undergoes an increment mainly due to fuselage bending. This is confirmed by the the different values predicted by Edge for the two ROMs built. The first difference to highlight relies in the \mathbf{Cm}_α derivative which is significantly affected by deformability effects. The solution predicted by MSC/NASTRAN almost reaches a null value, while SMARTCAD predicts even an inversion. On the other hand, the solution by Edge is still positive probably highlighting a benefic effect from the fuselage. Finally, considering the derivative \mathbf{CN}_δ the three solvers again agree on the general aeroelastic behavior for the aircraft considered. MSC/NASTRAN and SMARTCAD predict a coefficient tending to a null value, while for Edge the inversion has already occurred for this value of the dynamic pressure. This demands for a stiffening in fuselage bending. Indeed when mode n.9 is excluded from the modal base, the correction factor is still positive.

	Edge (ROM) $\alpha = \alpha_T$	SMARTCAD	MSC/NASTRAN
$\eta(\mathbf{CN}_\alpha)$	0.80	0.72	0.73
$\eta(\mathbf{Cm}_\alpha)$	0.31	-0.20	0.07
$\eta(\mathbf{CN}_\delta)$	-0.20	0.03	0.07
$\eta(\mathbf{Cm}_\delta)$	1.16	1.09	1.08

Table 22: Aeroelastic correction to steady longitudinal derivatives, $M_\infty = 0.65$, $z = 0$ m, deformable.

Conclusions

This work presented a software environment for aero-structural conceptual design, named NeoCASS, which allows to design the airframe once the geometrical configuration is defined. It is composed by different modules allowing the user to tackle all the aspects typical of aircraft conceptual design phase, starting from the initial weight and balance analysis, through the first structural sizing, till the final structural optimization. In particular the procedure includes a specific module, named SMARTCAD aiming at the aeroelastic analysis and optimization. After a synthesis of the capabilities offered by NeoCASS, a complete

case study, regarding the so-called TransCRuiser aircraft, is reported. Three different levels of validation of the results obtained with NeoCASS are reported, based on MSC/NASTRAN, a medium fidelity CFD tool and some available wind tunnel testing results, respectively.

Acknowledgements

Giampiero Bindolino and Paolo Mantegazza are acknowledged for the interesting discussions about Vortex Lattice Methods and the formulation of trim problems for linear aeroelasticity, while Andrea da Ronch for his initial contribution to the development of the GUESS module. A special thanks to Alessandro De Gaspari for the contribution to the GUI interface development and to Luca Riccobene for the implementation of W&B module. Alessandro Scotti is warmly acknowledged for his contribution to the TCR model design and manufacturing. The financial support by the European Commission through co-funding of the FP6 project SimSAC is acknowledged.

References

- ¹Raymer, D. P., *AIRCRAFT DESIGN: A Conceptual Approach, Fourth Edition*, AIAA Education Series, New York, NY, 2006.
- ²Torenbeek, E., *Synthesis of Subsonic Airplane Design*, Kluwer Academic Pub, Delft University Press, 1982.
- ³Lucia, D. J., "The SensorCraft Configurations: A Non-Linear AeroServoElastic Challenge for Aviation," *Proceedings of the 46th AIAA/ASME/ASCE/AHS/ASC SDM Conference*, Austin, Texas, 18 - 21 April 2005.
- ⁴Silva W. A., Vartio E., S. A. K. R. G. E. K. W. S. R., "Development of Aeroveloelastic Analytical Models and Gust Load Alleviation Control Laws of a SensorCraft Wind-Tunnel Model Using Measured Data," *Proceedings of the IFASD International Forum on Aeroelasticity*, Stockholm, June 17 - 20 2007.
- ⁵H., L. R., "Design of the BlendedWing Body Subsonic Transport," *Journal of Aircraft*, Vol. 41, No. 1, January-February 2004, pp. 1025.
- ⁶Antoine, N., Kroo, I., Willcox, K., and Barter, G., "A Framework for Aircraft Conceptual Design and Environmental Performance Studies," *Proceedings of the 10th AIAA/ISSMO Multidisciplinary Analysis and Optimization Conference*, Albany, New York, 30 August - 1 September 2004.
- ⁷Macci, S. H., "Semi-analytical method for predicting wing structural mass," Tech. rep., SAWE Paper No.2282, May 1995.
- ⁸Bindolino, G., Ghiringhelli, G., and Ricci, S., "Preliminary Sizing Of The Wing-Box Structure By Multi-Level Approach," *Int. Forum on Aeroelasticity and Structural Dynamics IFASD 2005, - Munich, Germany*, June 28 - July 01 2005.
- ⁹Ardema, M., Chambers, A., Hahn, A., Miura, H., and Moore, M., "Analytical Fuselage and Wing Weight Estimation of Transport Aircraft," Tech. Rep. 110392, NASA, Ames Research Center, Moffett Field, California, May 1996.
- ¹⁰Mason, W. H., "http://www.aoe.vt.edu/~mason/Mason_f/MRsoft.html/," LDSTAB software, last accessed 2009.
- ¹¹Shanley, F. R., *Weight-strength analysis of aircraft structures*, Dover Publications, Inc., New York, 2nd ed., 1960.
- ¹²Crawford, R. F. and Burns, A. B., "Minimum weight potentials for stiffened plates and shells," *AIAA Journal*, Vol. 1, No. 4, 1963, pp. 879-886.
- ¹³Moran, J., *An Introduction to Theoretical and Computational Aerodynamics*, John Wiley & Sons, 1984.
- ¹⁴Katz, J. and Plotkin, A., *Low-Speed Aerodynamics From Wing Theory to Panel Methods*, McGraw-Hill series in Aeronautical and Aerospace Engineering, 1991.
- ¹⁵Albano, E. and Rodden, W. P., "A Doublet-Lattice Method for Calculating the Lift Distributions on Oscillating Surfaces in Subsonic Flow," *AIAA Journal*, Vol. 7, No. 2, 1969, pp. 279-285.
- ¹⁶Chen, P. C. and Liu, D. D., "A Harmonic Gradient Method for Unsteady Supersonic Flow Calculations," *Journal of Aircraft*, Vol. 22, No. 15, 1985, pp. 371-379.
- ¹⁷Ghirghelli, G. L., Masarati, P., and Mantegazza, P., "A Multi-Body Implementation of Finite Volume Beams," *AIAA Journal*, Vol. 38, No. 1, January 2000, pp. 131-138.
- ¹⁸Quaranta, G., Masarati, P., and Mantegazza, P., "A Conservative Mesh-free Approach for Fluid-Structure Interface Problems," *International Conference on Computational Methods for Coupled Problems in Science and Engineering*, edited by M. Papadrakakis, E. Oñate, and B. Schrefler, CIMNE, Santorini, Greece, 2005.

- ¹⁹Beckert, A. and Wendland, H., "Multivariate Interpolation for Fluid-Structure-Interaction Problems Using Radial Basis Functions," *Aerospace Science Technology*, Vol. 5, 2001, pp. 125–134.
- ²⁰Haftka, R. T. and Gürdal, Z., *Elements of structural optimization*, Dordrecht, 3rd ed., 1992.
- ²¹Bennet, R. and Edwards, J., "An overview of recent developments in computational aeroelasticity," *Proceedings of the 29th AIAA Fluid Dynamics Conference, (Albuquerque, NM)*, Seattle, WA, 15–18 June 1998.
- ²²Karpel, M., Yaniv, S., and Livshits, D. S., "Integrated Solution for Computational Static Aeroelasticity of Rockets," *Journal of Spacecraft and Rockets*, Vol. 35, No. 5, September–October 1998, pp. 612–618.
- ²³Milne, R. D., "Some remarks on the dynamics of deformable bodies," *AIAA Journal*, Vol. 6, No. 3, March 2000, pp. 556–5582.
- ²⁴Zink, P. S., Mavris, D. N., and Raveh, D. E., "Maneuver Trim Optimization Techniques for Active Aeroelastic Wings," *Journal of Aircraft*, Vol. 38, No. 6, 2001, pp. 1139–1146.
- ²⁵Raveh, D. E., "Maneuver Load Analysis of Overdetermined Trim Systems," *Journal of Aircraft*, Vol. 45, No. 1, 2008, pp. 119–129.
- ²⁶Kelley, C., *Iterative methods for linear and nonlinear equations*, SIAM, Philadelphia, PA, 1995.
- ²⁷Cavagna, L., Quaranta, G., Mantegazza, P., and Marchetti, D., "Aeroelastic Assessment of the Free Flying Aircraft in transonic regime," *International Forum on Aeroelasticity and Structural Dynamics IFASD-2007*, Stockholm, Sweden, June 18–20, 2007.
- ²⁸Michler, A. K., Dwight, R. P., and Heinrich, R., "Trimmed Simulation of a Transport Aircraft using Fluid-Structure Coupling," *International Conference on Computational Methods for Coupled Problems in Science and Engineering*, Ischia, Italy, June 8 – 11 2009.
- ²⁹Cavagna, L., Ricci, S., and Scotti, A., "Active Aeroelastic Control over a four control Surface Wind Tunnel Wing Model," *International Forum on Aeroelasticity and Structural Dynamics IFASD-2007*, Stockholm, Sweden, June 18–20, 2007.
- ³⁰Cavagna, L., Masarati, P., and Quaranta, G., "Fluid-structure interaction for maneuvering aircraft using a CFD/Multibody combined approach," *International Forum on Aeroelasticity and Structural Dynamics*, Seattle, WA, June 22 – 25 2009.
- ³¹Raveh, D. E., Karpel, M., and Yaniv, S., "Nonlinear Design Loads for Maneuvering Elastic Aircraft," *Journal of Aircraft*, Vol. 37, No. 4, 2000, pp. 313–318.
- ³²Zink, P. S., Raveh, D. E., and Mavris, D. N., "An Integrated Trim and Structural Design Process for Active Aeroelastic Wing Technology," *Proceedings of the 42nd AIAA/ASME/ASCE/AHS/ASC Structures, Structural Dynamics, and Materials Conference and Exhibit*, Seattle, WA, 16–19 April 2001.
- ³³Rodden, W. and Love, J., "Equations of Motion of a Quasisteady Flight Vehicle Utilizing Restrained Static Aeroelastic Characteristics," *Journal of Aircraft*, Vol. 22, No. 3, 1985, pp. 802–809.
- ³⁴Fisher, C. and Arena, A., "On The Transpiration Method For Efficient Aeroelastic Analysis Using An Euler Solver," *Proceedings of the AIAA Atmospheric Flight Mechanics Conference*, San Diego, CA, July 29–31 1996.
- ³⁵Cavagna, L., Quaranta, G., and Mantegazza, P., "Application of Navier-Stokes simulations for aeroelastic assessment in transonic regime," *Computers & Structures*, Vol. 85, No. 11-14, 2007, pp. 818–832, Fourth MIT Conference on Computational Fluid and Solid Mechanics.